A sea state dependent spume generation function

James A. Mueller* & Fabrice Veron

College of Marine and Earth Studies,

University of Delaware, Newark, DE, USA

*Corresponding author address: James A. Mueller, College of Marine and Earth Studies, University of Delaware, 210 Robinson Hall, Newark, DE 19716.

E-mail: jmueller@udel.edu

ABSTRACT

The uncertainty of the sea spray generation function continues to obscure spray-mediated momentum and scalar fluxes, especially for intense wind conditions. Most previous studies assume a constant form (spectral shape) for the droplet distribution, even though a shift to smaller drops with increased wind forcing is expected. In this paper, a new generation function for spume drops is derived, but unlike previous studies, both its form and magnitude change with wind forcing. Fairly good agreement between this spume generation function and the limited data available is found. A potential explanation for the vast size differences between previous spume generation studies is also provided by distinguishing the drops formed at the surface from the drops transported vertically where measurements are routinely made.

1. Introduction

Current hurricane models are unable to produce high wind speeds when using traditional air-sea flux parameterizations. Emanuel (1995) showed that the ratio of the enthalpy exchange coefficient to the drag coefficient controls the maximum wind speed and that traditional parameterizations produce too low of a ratio when extrapolated to high wind speeds. Consequently, some combination of a higher enthalpy exchange coefficient and a lower drag coefficient is necessary to simulate hurricanes in models. Such uncertainty indicates that our knowledge of these coefficients, which are largely based on data-based empirical formulae at lower wind speeds, do not extrapolate to high wind speed conditions in the field. While the drag coefficient seems to depart from previous extrapolated estimates at high wind speeds as seen in both laboratory and field experiments (Donelan et al. 2004; Powell et al. 2003), the behavior of the enthalpy coefficient remains largely unknown. Without a strong reduction of the drag coefficient, even a slightly increasing enthalpy exchange coefficient cannot constitute a sufficiently high coefficient ratio. Sea spray has the potential not only to increase the enthalpy exchange coefficient dramatically but also to decrease the drag coefficient at high winds. Numerous studies have examined the impact of sea spray on the drag and enthalpy fluxes (e.g. Edson and Fairall 1994; Andreas 1998; Pattison and Belcher 1999; Meirink 2002), but no clear consensus exists.

The great uncertainty of the sea spray source function ultimately leads to unresolved spray-mediated momentum, heat and mass fluxes. Spume droplets, which form when the wind tears water globules from the crest of breaking waves, presumably dominate the sea spray problem at high wind speeds due to their relative size. Yet, very little is known

about the production of spume droplets. Most previous studies have assumed a constant form, found empirically, for the sea spray generation function with increased wind forcing. Various theoretical models for droplet distributions in a turbulent carrier fluid (e.g. Hinze 1955), however, predict a reduction of the mean diameter with wind speed. If the droplet distribution does indeed shift to smaller droplets as predicted, the amount of wind energy necessary to produce each unit mass of spray increases. Andreas et al. (1995) argue that the energy required to work against surface tension and form droplets roughly scales as the wind energy flux into the ocean. Thus, the amount of mass produced relative to the wind energy does not necessarily increase.

Herein we present a semi-empirical derivation of the spume source function. Section 2 provides a general overview of a plausible mechanism for the generation and break-up of ligaments and spume drops. We use experimental data of single ligament formation events from round water jets along with an estimate of event occurrences at the air-sea interface (given in section 3) to find the spume generation function, which consequently spans a wider range of sizes than most previous functions. With the inclusion of large drops, we also consider the vertical transport and suspension of the produced drops after formation in section 4. Finally, in section 5 we compare the corresponding mass and energy fluxes of our source function with previous studies.

2. Spume production process

Instead of assuming that the droplet distribution at a given height is produced instantaneously, we consider a possible spume production process. From wind-wave experiments

(Koga 1981) as well as experiments investigating the break-up of a liquid sheet (e.g. Ahmed et al. 2008; Li and Ashgriz 2006) and a round water jet (Lasheras et al. 1998; Marmottant and Villermaux 2004), the following mechanism for spume production is proposed. The shear between the light, fast-moving air and the heavy, slow-moving water produces (Kelvin-Helmholtz[1]) instabilities. Subsequently, a secondary instability, transverse to the wind, develops. The wind elongates these modulations to form coherent ligaments, which are eventually torn away from the surface, forming globules. These globules, after initial coalescence, are subject to fragmentation by shear forces and by turbulent fluctuations.

While there may be additional coalescence along the way, the equilibrium state ultimately consists of the stable, fully broken-up (atomized) droplets (Pilch and Erdman 1987). Moreover, some of the largest globules fall back to the ocean before being fully atomized. The ultimate formation process is not of critical importance here because we use empirical relationships, but we note here that discrepancies between previous estimates and measurements of the sea spray source function might stem from the fact that the equilibrium distribution is not reached instantaneously. Any empirical sea spray generation function found above the surface (e.g. Wu 1993; Andreas 1992) will most likely be closer to the atomized distribution that is transported vertically, while investigations of the production process (e.g. Anguelova et al. 1999; Koga 1981) will more closely resemble the globule distribution.

[1]To the best of the authors' knowledge, Owen M. Phillips (1969) was the first to speculate that spume droplets originate from a Kelvin-Helmholtz instability.

a. Ligament formation

The ligament-mediated spray relationships are derived from those found in the round water jet studies because full droplet distributions are unavailable for wind-wave and liquid sheet experiments of ligament-mediated spray. From Marmottant and Villermaux (2004)[2], the average diameter of a ligament, ξ, and the transverse spacing between ligaments, $\lambda_\perp$, are powers of the interfacial Weber number, $We_\delta = \rho_a u_a^2 \delta/\sigma$:

$$\begin{aligned} \xi &= 4.367 \times 10^{-3}\ \delta \left(We_\delta \rho_a/\rho_w\right)^{-1} \\ \lambda_\perp &= 3.467\delta \left(We_\delta \rho_a/\rho_w\right)^{-1/3}, \end{aligned} \tag{1}$$

where ρ is the density, u the velocity, $\delta = u_a/(du_a/dz)|_{max}$ the vorticity thickness and σ the surface tension. The subscripts, 'a' and 'w', denote the air and water phases, respectively. The air velocity relative to the surface is roughly $u_a = U_{10} - U_0$, where U is the mean velocity and the subscripts 10 and 0 denote 10-m and surface heights, respectively. The maximum velocity gradient is taken as $du_a/dz|_{max} \approx u_*^2/\nu_a$, where ν_a is the kinematic viscosity of air. Finally, the diameter of a sphere with the equivalent volume as the average ligament, D_0, is found to be a constant multiple of the vorticity thickness, $D_0 = 4.334\delta$.

[2]The coefficients and power laws presented here may differ slightly from those given in Marmottant and Villermaux (2004) because we use least-square fits to their air-water data.

b. Atomization

The volume of water from each ligament gets broken up further into spray. The vertically transported spray is the distribution that most empirical sea spray studies measure. Marmottant and Villermaux (2004) found that for a round water jet the mean diameter of the resulting, atomized spray is roughly a constant fraction of the volume equivalent diameter of the average ligament, $\bar{D} \approx 0.4 D_0$. They also found that these droplets follow a gamma distribution:

$$p(x) = n^n x^{n-1} e^{-nx} / \Gamma(n), \tag{2}$$

where $x = D/\bar{D}$ is the normalized drop diameter. For this gamma distribution, the mean is 1 and the variance is n^{-1}. According to Villermaux et al. (2004), n, between 2 and 4 for their data, increases slightly with wind speed and is a function of the ratio, $\bar{D}/\xi$, taken here to be

$$n = 0.4(\bar{D}/\xi) + 2. \tag{3}$$

Consequently, the variance of the drop distribution with normalized diameter decreases slightly as the wind forcing increases. Also, to conserve volume, the drop distribution is rescaled as

$$\frac{dN_l}{dD} = \frac{D_0^3}{\int p(D/\bar{D}) D^3 dD} p(D/\bar{D}). \tag{4}$$

We now compare both the ligament and characteristic spray diameters with those expected from general break-up processes. As mentioned earlier, there are two mechanisms for the atomization of globules into spray: shear break-up and turbulent break-up. Shear break-up occurs if the droplet diameter produces a shear Weber number greater than the

critical shear Weber number:

$$We_s = \rho_a v_s^2 D/\sigma > We_s|_{crit}, \tag{5}$$

where v_s is the slip velocity between the droplet and the air flow. This defines a maximum stable diameter of the order

$$D_s = We_s|_{crit}\sigma v_s^{-2}/\rho_a. \tag{6}$$

First, consider a falling droplet in a quiescent carrier fluid. The maximum slip velocity is the terminal velocity of the drop. Due to regimes of high Reynolds numbers and shape deformation, the fall velocity is not equivalent to the Stokes' terminal velocity (accounting for the added mass) for larger droplets. Instead the settling velocity is taken to be

$$v_f(D) = \frac{D^2 g(\rho_w - \rho_a)}{18\rho_a \nu_a f}, \tag{7}$$

with droplet Reynolds number $Re_d(D) = D\sqrt{v_s^2}/\nu_a$ and the correction Stokes' flow, $f = f_C f'$, where

$$f_C = 1 + 0.15Re_d^{0.687} + \frac{0.0175}{1 + 4.25 \times 10^4 Re_d^{-1.16}} \tag{8}$$

is the high Reynolds number correction for solid particles from Clift and Gauvin (1970) and

$$f' = \left[0.1024 + \frac{0.8976Re_d^{-2.3}}{2472^{-2.3} + Re_d^{-2.3}}\right]^{-1} \tag{9}$$

is the shape deformation correction for very large water droplets. Hinze (1949) found that the critical Weber number for a falling droplet is approximately 22. Now consider a falling droplet in a turbulent flow where the critical shear Weber number can be closer to 10 (Wierzba 1990). In this case, the maximum slip velocity is $v_s = \sqrt{\sigma_x^2 + v_f^2}$, where σ_x is the standard deviation of the horizontal air velocity.

Similarly, turbulent break-up occurs if the turbulent Weber number exceeds the critical turbulent Weber number:

$$We_t = \rho_a \overline{u'_a(D)^2} D/\sigma > We_t|_{crit}, \tag{10}$$

where $\overline{u'_a(D)^2}$ is the mean square of the fluctuating velocities on the two ends of the droplet. Hinze (1955) found the critical turbulent Weber number to be 0.585. Assuming local isotropy at the droplet length scale, the critical turbulent Weber number is

$$We_t|_{crit} = \frac{\rho_a D_t}{\sigma} \left(\epsilon D_t\right)^{2/3} = 0.585, \tag{11}$$

where ϵ is the mean turbulent kinetic energy (TKE) dissipation rate and the corresponding maximum stable diameter, defined as the diameter for which 95% by volume is contained in drops with $D \leq D_t$, is

$$D_t = 0.725(\sigma/\rho_a)^{3/5} \epsilon^{-2/5}. \tag{12}$$

The TKE dissipation rate in the wave boundary layer is not equivalent to the mean shear production (Hara and Belcher 2004). Instead, the TKE balance, outside the viscous sublayer, is

$$\epsilon = u_*^2 \frac{dU}{dz} + B_p + \frac{d\Pi}{dz}, \tag{13}$$

where $\kappa \approx 0.4$ is the von Karman constant, B_p is the production/destruction of TKE due to buoyancy, and $d\Pi/dz$ is the divergence of the wave-induced energy flux (Mueller and Veron 2009a; Hara and Belcher 2004). The air-sea momentum flux is defined as $\tau = \rho_a u_*^2$ and is modeled according to (Mueller and Veron 2009b).

Figure 1 plots the mean volume equivalent diameter for each ligament, D_0, as well as the maximum diameter in the resulting spray, defined as the diameter at which 95% by

volume is contained within smaller drops, $D_{95\%}$. The theoretical maximum stable diameters from the critical shear and turbulent Weber numbers are also given. Because the dissipation changes with height above the surface, a constant near-surface height, which is equivalent to the peak radius at $U_{10} = 15$ m s^{-1} and lies outside the viscous sublayer for all wind speeds greater than 15 m s^{-1}, is used for the calculation of the TKE dissipation rate. For reference, the distribution peaks from figure 3 of Anguelova et al. (1999) are plotted at their 10-m equivalent wind speed. Immediately after initial coalescence upon separation from the surface but before atomization, these elliptical globules are of a similar size. The wind speed dependence of the maximum droplet diameter characteristically follows the maximum diameter derived from the critical turbulent Weber number, D_t (Hinze 1955). Although drops that are larger than those predicted to be stable by theoretical diameter maxima can exist in the flow for some finite amount of time before break up, all vertically transported drops appear to be stable. This can be seen from the maximum droplet size, D_f, that the turbulence can transport vertically, and it will be discussed further in section 4.

3. Source function

We assume that the spume production process occurs above the crest of actively breaking waves. Phillips (1985) defined the length of breaking crests of incremental wave speed $d\mathbf{c}$ per unit area to be $L(\mathbf{c}) = \Lambda(\mathbf{c})d\mathbf{c}$, where $\Lambda(\mathbf{c})$ is the spectral length per unit area. To find L, we use the two-dimensional empirical wave spectrum (and wave age-fetch dependence) from Elfouhaily et al. (1997) coupled with the surface stress model from Mueller and Veron (2009b) with the implicit assumption that the wind and waves are in equilibrium, i.e. the

spectral dissipation due to breaking is equivalent to the spectral wind energy input. The corresponding area swept by breaking wave crests of incremental wave speed $d\mathbf{c}$ per unit area per unit time is $A = \mathbf{c}\Lambda(\mathbf{c})d\mathbf{c}$. From this area, the active whitecap coverage can be modeled as

$$W = \int T_b \mathbf{c}\Lambda(\mathbf{c})d\mathbf{c}, \tag{14}$$

where T_b is the active breaking time and is proportional to the wave period, T (Rapp and Melville 1990; Phillips et al. 2001; Melville and Matusov 2002). The active breaking time lies somewhere in the range $0.1T$ to T. Using these values, the corresponding whitecap A coverage values fall in the conventional range (see figure 1 in Anguelova and Webster, 2006). The lowest reported white cap coverage data seem to be that from Monahan and Woolf (1989), and when matched to equation 14, we find $T_b < 0.1T$, which seems rather low. Thus, we take $T_b \approx 0.2T$ hereafter, which produces a whitecap A coverage roughly equivalent to that reported in Monahan (1993).

With the active breaking time and spectral whitecap coverage, dW, the total length of breaking wave crests per unit area per unit time is $L_{sp} = \int \lambda_b^{-1} T_b^{-1} dW$, or

$$L_{sp} = \int \frac{\mathbf{c}}{\lambda_b}\Lambda(\mathbf{c})d\mathbf{c}, \tag{15}$$

where the breaking length is $\lambda_b = T_b\mathbf{c}$.

Because spume production presumably occurs at the crests of actively breaking waves, this new length, L_{sp}, provides the length of spume production sites per unit area per unit time. The number of ligaments formed per unit area per unit time can now be found from the length of spume production sites divided by the transverse spacing between ligaments

(equation 1),

$$n_l = L_{sp}/\lambda_{\perp}. \tag{16}$$

Finally, the spume source function, which is a function of both wind speed and fetch, is

$$\frac{dN}{dD} = n_l \frac{dN_l}{dD}, \tag{17}$$

and by substitution can be expressed in more familiar variables as,

$$\frac{dN}{dD} = \frac{23.481\left(U_{10}-U_0\right)^2 \nu_a^2}{u_*^4 \int p(D/\bar{D}) D^3 dD} \left(\frac{\rho_a^2 \nu_a \left|U_{10}-U_0\right|^3}{\rho_w \sigma u_*^2}\right)^{1/3} \int \frac{\mathbf{c}}{\lambda_b} \Lambda(\mathbf{c}) d\mathbf{c}\; p(D/\bar{D}), \tag{18}$$

where $p(D/\bar{D})$ is the gamma distribution defined by equations 2 and 3. The volume associated with these droplets is

$$\frac{dV_N}{dD} = \frac{\pi D^3}{6} \frac{dN}{dD}. \tag{19}$$

Figures 2a and 2c respectively plot the spume surface production function for multiple 10-m wind speeds at a laboratory scale fetch (22 m) and a field scale fetch (75 km). The peaks of our distributions give somewhat smaller droplet diameters than those reported by Anguelova et al. (1999), given in Figure 1. This discrepancy could be due to their imaging limitations; the resolution of their images was roughly 1 mm. As noted previously, the distribution peaks show more droplets and smaller peak radii with increasing wind speed. The corresponding volume production functions in figure 2b and 2d show that the peaks of the volume distribution only shift upward slightly with wind speed. The effect of transitioning to smaller droplets suggests that the additional energy from increased wind forcing primarily goes to the atomization of the droplets rather than to the increase of volume/mass production.

Figure 3 plots the total production rate of spume drops at both laboratory and field fetches. For direct comparison to the spume components of previous spray generation functions, the lower integration limit for the diameter is 100 μm, which is just above the jet droplet range (6–100 μm Andreas 1998). Note that the lower limit for the Wu (1993) function is 150 μm. From our model, the total production of spume drops seems to be slightly less at a laboratory fetch. This is a result of less normalized breaking relative to the 75 km fetch.

In the limit that every dominant wave crest breaks, the length of breaking crests per unit area per unit time depends only on the number of crests that pass through a unit area per unit time. As the dominant waves get longer with increasing fetch, the corresponding phase speeds only increase as the square root of the wave length, according to the deep water dispersion relationship. In other words, the number of crests passing though a unit area per second is greater at shorter fetches. This means that there must be more normalized breaking at the 75 km fetch. Otherwise, there would be more spume production at the 22 m fetch.

Nevertheless, the wind speed dependence of our spume production function follows the function from Fairall et al. (1994) at all wind speeds but is about an order of magnitude lower. This discrepancy in magnitude likely stems from the difference between whitecap A and whitecap B coverages. Whereas Fairall et al. (1994) find the magnitude from whitecap B coverage, our model is tuned with whitecap A coverage because spume drops presumably form only at active breaking sites. Furthermore, our generation function does not consider jet and film spray droplets that can form within the more expansive whitecap B coverage.

4. Vertical flux

Although the source function presented here produces smaller droplets than those found in laboratory experiments of the spume generation process (Anguelova et al. 1999), it predicts much larger droplets than those found in laboratory and field experiments farther away from the production sites. Essentially, the largest drops never get suspended in the air because they are too heavy to be transported vertically. The balance between the gravitational acceleration and maximum vertical acceleration from the turbulent air flow dictates the upward flux of droplets. Accordingly, the maximum suspended diameter shown in figure 1 is the diameter at which $v_f(D_f) = 2\sigma_z$, where $\sigma_z = 1.25u_*$ is the standard deviation of the turbulent vertical velocity. Assuming the distribution of the turbulent vertical velocity is Gaussian, a simple probabilistic relationship between the produced droplets and the vertically transported droplets is the complementary error function ($erfc$) of the ratio between the settling velocity and the standard deviation of vertical turbulent velocity. As this ratio goes to zero, $erfc$ goes to one. When the settling velocity is greater than two standard deviations of the turbulent velocity, $erfc$ quickly goes to zero. In other words, all of the droplets with settling velocities greater than the most extreme upward turbulent velocities immediately fall back to the ocean, while nearly all of the droplets with very small settling velocities are able to be suspended. The resulting distribution of drops transported upward takes the following form:

$$\frac{dF}{dD} = erfc\left(v_f(D)/\sigma_z\right)\frac{dN}{dD}, \tag{20}$$

with corresponding volume flux,

$$\frac{dV}{dD} = \frac{\pi D^3}{6}\frac{dF}{dD}. \tag{21}$$

Figures 2a and 2c show the vertically transported distribution of spume for both laboratory and field fetches, and figures 2b and 2d plot the corresponding volume flux. For reference, a line with the typical diameter relationship, D^{-8} (e.g. Andreas 1992; Fairall et al. 1994; Wu 1993), for large drops is also plotted. Compared to the source functions, the peak diameter of the vertically transported spray does not shift nearly as much with wind speed. In fact, the peaks in figure 2 show that the diameter of the vertically transported spray increases with wind speed until the wind reaches roughly $30ms^{-1}$; at greater wind speeds, the peak diameter reduces as before. The average value for these peaks of the vertically transported spray is roughly 300 μm, which agrees with the peaks of the spume functions reviewed by Andreas (2002). Nevertheless, figure 2 illustrates a possible reason why previous investigations have found or assumed a constant peak diameter even though theoretical studies predict smaller droplets with increased wind forcing.

5. Mass and energy fluxes

So far we have only considered the distribution of spume droplets. We will now investigate the total mass and energy fluxes from these distributions. The respective produced and suspended mass fluxes can easily be found through integration as

$$M_N = \rho_w \int \frac{dV_N}{dD} dD$$
$$M = \rho_w \int \frac{dV}{dD} dD. \tag{22}$$

Figure 4 plots the mass fluxes for the source and suspended distributions as a function of modeled friction velocity. For reference, the mass fluxes of spray functions from Andreas

(1998), Fairall et al. (1994) and Wu (1993) are also shown. The integration limits of equation 22 are 40 μ m and 10 mm. While the lower limit is a conventional number, the upper limit is roughly the maximum diameter at $U_{10} = 9$ m s^{-1}, where spume production begins as can be seen in figure 1. The mass of spume droplets produced at the surface appears to be nearly constant with wind forcing. Again this is because of the balance between decreasing droplet size and increasing number of drops formed with increased wind forcing. This balance will be explored in more detail below.

The mass of spume droplets that can be suspended, however, increases sharply with wind forcing at low to moderate wind forcing. Eventually, the wind forcing becomes sufficiently strong to suspend virtually all of the droplets produced. Therefore, even the mass of suspended drops plateaus at extremely high wind speeds. An upper limit for mass production is somewhat intuitive because there is only so much surface from which to tear water. In fact, the spray function from Fairall et al. (1994) scales the normalized Andreas (1992) spray function at $U_{10} = 11$ m s^{-1} with whitecap B coverage. This leads to the maximum mass flux, i.e. where the whitecap B coverage is 100%, at approximately $U_{10} = 40$ m s^{-1} or $u_* = 2$ m s^{-1}. The limit of the mass flux for our source function at high wind forcing is about four times lower than the limit from Fairall et al. (1994) also plotted in figure 4 (gray dashed line), which again roughly corresponds to the difference between whitecap coverages A and B. In any event, our two curves provide natural bounds for previous spume production functions. The spume source function (upper curve) represents the drops that are generated just above the crest of breaking waves, some of which may never be seen as they never separate substantially from the surface. The suspended spume function (lower curve) represents the droplets that can be suspended in the air. The spume distribution that resides in the air for

some finite amount of time lies somewhere between these two curves.

The nearly constant mass flux with wind forcing as shown in figure 4 warrants further exploration. The reduction of droplet sizes with wind forcing could potentially mean that additional wind energy breaks droplets apart rather than suspends more water mass. Additional wind energy could further go into the potential and kinetic energy of the drops through more net vertical transport. Regarding the formation of smaller droplets, Andreas et al. (1995) found that the energy required to form the extra surface area is the free energy of the created spume drops. The time rate of change of free energy per unit of sea surface area is

$$E_N = \frac{1}{3}\sigma\pi \int D^2 \frac{dN}{dD} dD. \tag{23}$$

Substitute dF/dD for dN/dD to find the vertically transported energy flux, E. The integration limits are the same as those in the mass flux calculation. Figure 5 shows the energy flux for the spume source function and the suspended spume function. For reference, the energy fluxes from Andreas (1998), Fairall et al. (1994) and Wu (1993) are also shown. Again, the limit of our energy flux at high wind speeds is about three times lower than the limit from Fairall et al. (1994) because of the difference between whitecap A coverage and whitecap B coverage. This also may explain the slope of our energy flux, as we do not consider the smaller jet and film droplets that result from whitecap B coverage. Moreover, the extrapolated energy flux from Andreas (1998) does not increase at the rate of energy supplied from the wind to the ocean at high values of friction velocity because our modeled friction velocity increases linearly with wind speed at high winds. Even though the mass flux of our source function plateaus, the shift to smaller droplets results in more free energy with increased

wind forcing.

The rate at which the wind provides energy to the surface, $E_t \propto \alpha\tau U_0 \propto \beta u_*^3$, is also plotted in figure 5, where the surface drift velocity is approximated as $U_0 \approx 15.2\,(\tau_\nu/\rho_w)^{1/2}$ (Wu 1983) with τ_ν the average viscous stress per unit area from Mueller and Veron (2009b). To match E_t with E_N and E at high wind speeds, α and β are $\sigma/150$ and $\alpha/10$, respectively. From such small values, it is evident that much of the energy supplied to the surface does not appear to go toward generating spume droplets. Whitecap formation and other wave breaking processes presumably consume the rest of the energy when the air-sea boundary is close to equilibrium. Furthermore, the formation energy required to produce the source distribution of drops is presumably less significant than the energy required to form the suspended droplets. The reason is that the suspended droplets not only take mechanical energy at formation but also consume heat energy as they evaporate and get even smaller.

6. Conclusions

The proposed spume generation process produces drop sizes that span the empirical range. Immediately after separation from the surface, the spume drops have diameters on the order $0.1 - 7\ mm$. The vertically transported and completely atomized drops are closer to the more familiar $10 - 500\ \mu m$ range. Although the proposed source function implies considerably larger mass and energy fluxes at low to moderate wind speeds, most of this discrepancy is due to its vast size range compared to other source functions. Excluding the drops greater than 1.5 mm in diameter, which are typically ignored because they cannot be transported vertically, our source function closely resembles currently accepted generation

functions. The uncertainty in many of the terms stresses the need for further study of the individual processes presented here as well as direct measurements of the production and suspension of droplets.

Acknowledgments.

We thank Ed Andreas for numerous fruitful discussions as well as his helpful suggestions on an early draft. This work was supported by ONR grant (N00014-05-1-0609) to Veron.

REFERENCES

Ahmed, M., A. Amighi, N. Ashgriz, and H. N. Tran, 2008: Characteristics of liquid sheets formed by splash plate nozzles. *Exp. Fluids*, **44**, 125–136, doi:10.1007/s00348-007-0381-4.

Andreas, E. L., 1992: Sea spray and the turbulent air-sea heat fluxes. *J. Geophys. Res.*, **97 (C7)**, 11 429–11 441.

Andreas, E. L., 1998: A new sea spray generation function for wind speeds up to 32m s^{-1}. *J. Phys. Oceanogr.*, **28 (11)**, 2175–2184.

Andreas, E. L., 2002: A review of the sea spray generation function for the open ocean. *Atmosphere-Ocean Interactions*, W. A. Perrie, Ed., WIT Press, Southhampton, UK, Vol. 1, 1–46.

Andreas, E. L., J. B. Edson, E. C. Monahan, M. P. Rouault, and S. D. Smith, 1995: The spray contribution to net evaporation from the sea: a review of recent progress. *Bound.-Layer Meteor.*, **72 (1-2)**, 3–52.

Anguelova, M., R. P. Barber, and J. Wu, 1999: Spume drops produced by the wind tearing of wave crests. *J. Phys. Oceanogr.*, **29**, 1156–1165.

Anguelova, M. D. and F. Webster, 2006: Whitecap coverage from satellite measurements: A first step toward modeling the variability of oceanic whitecaps. *J. Geophys. Res.*, **111 (C3)**, doi:10.1029/2005JC003158.

Clift, R. and W. H. Gauvin, 1970: The motion of particles in turbulent gas streams. *Proc. Chemeca'70*, **1**, pp. 14.

Donelan, M. A., B. K. Haus, N. Reul, W. J. Plant, M. Stiassnie, H. C. Graber, O. B. Brown, and E. S. Saltzman, 2004: On the limiting aerodynamic roughness of the ocean in very strong winds. *Geophys. Res. Lett.*, **31 (18)**, doi:10.1029/2004GL019460.

Edson, J. B. and C. W. Fairall, 1994: Spray droplet modeling. 1. Lagrangian model simulation of the turbulent transport of evaporating droplets. *J. Geophys. Res.*, **99 (C12)**, 25 295–25 311.

Elfouhaily, T., B. Chapron, K. Katsaros, and D. Vandemark, 1997: A unified directional spectrum for long and short wind-driven waves. *J. Geophys. Res.*, **102 (C7)**, 15 781–15 796.

Emanuel, K. A., 1995: Sensitivity of tropical cyclones to surface exchange coefficients and a revised steady-state model incorporating eye dynamics. *J. Atmos. Sci.*, **52 (22)**, 3969–3976.

Fairall, C. W., J. D. Kepert, and G. J. Holland, 1994: The effect of sea spray on surface energy transports over the ocean. *Global Atmos. Ocean Syst.*, **2**, 121–142.

Hara, T. and S. E. Belcher, 2004: Wind profile and drag coefficient over mature ocean surface wave spectra. *J. Phys. Oceanogr.*, **34 (11)**, 2345–2358.

Hinze, J. O., 1949: Critical speeds and sizes of liquid globules. *App. Sci. Res.*, **A1 (4)**, 273–288.

Hinze, J. O., 1955: Fundamentals of the hydrodynamic mechanism of splitting in dispersion processes. *A.I.Ch.E.J.*, **1 (3)**, 289–295.

Koga, M., 1981: Direct production of droplets from breaking wind-waves-its observation by a multi-colored overlapping exposure photographing technique. *Tellus*, **33**, 552–563.

Lasheras, J. C., E. Villermaux, and E. J. Hopfinger, 1998: Break-up and atomization of a round water jet by a high-speed annular air jet. *J. Fluid Mech.*, **357**, 351–379.

Li, R. and N. Ashgriz, 2006: Characteristics of liquid sheets formed by two impinging jets. *Phys. Fluids*, **18**, 087 104, doi:10.1063/1.2338064.

Marmottant, P. H. and E. Villermaux, 2004: On spray formation. *J. Fluid Mech.*, **498**, 73–111, doi:10.1017/S0022112003006529.

Meirink, J., 2002: The role of wind-waves and sea spray on air-sea interaction. PhD dissertation, Technische Universiteit Delft, 161 pp.

Melville, W. K. and P. Matusov, 2002: Distribution of breaking waves at the ocean surface. *Nature*, **417**, 58–63.

Monahan, E. C., 1993: Occurrence and evolution of acoustically relevant subsurface bubble plumes and their associated, remotely monitorable, surface whitecaps. *Natural Physical Sources of Underwater Sound*, B. R. Kerman, Ed., Kluwer, 503–517.

Monahan, E. C. and D. K. Woolf, 1989: Variations of whitecap coverage with Wind stress and water temperature – Comments. *J. Phys. Oceanogr.*, **19 (5)**, 706–709.

Mueller, J. A. and F. Veron, 2009a: A lagrangian stochastic model for heavy particle dispersion in the atmospheric marine boundary layer. *Bound.-Layer Meteor.*, **130 (2)**, 229–247, doi:10.1007/s10546-008-9340-8.

Mueller, J. A. and F. Veron, 2009b: Nonlinear formulation of the bulk surface stress over breaking waves: feedback mechanisms from air-flow separation. *Bound.-Layer Meteor.*, **130 (1)**, 117–134, doi:10.1007/s10546-008-9334-6.

Pattison, M. J. and S. E. Belcher, 1999: Production rates of sea-spray droplets. *J. Geophys. Res.*, **104 (C8)**, 18 397–18 407.

Phillips, O. M., 1969: *Dynamics of the Upper Ocean*. Cambridge University Press, 261 pp.

Phillips, O. M., 1985: Spectral and statistical properties of the equilibrium range in wind-generated gravity waves. *J. Fluid Mech.*, **156**, 505–531.

Phillips, O. M., F. L. Posner, and J. P. Hansen, 2001: High range resolution radar measurements of the speed distribution of breaking events in wind-generated ocean waves: Surface impulse and wave energy dissipation rates. *J. Phys. Oceanogr.*, **31 (2)**, 450–460.

Pilch, M. and C. A. Erdman, 1987: Use of breakup time and velocity history data to predict the maximum size of stable fragments for acceleration-induced breakup of a liquid-drop. *Int. J. Multiphase Flow*, **13 (6)**, 741–757.

Powell, M. D., P. J. Vickery, and T. A. Reinhold, 2003: Reduced drag coefficient for high wind speeds in tropical cyclones. *Nature*, **422**, 279–283, doi:10.1038/nature01481.

Rapp, R. J. and W. K. Melville, 1990: Laboratory measurements of deep-water breaking waves. *Phil. Trans. R. Soc. Lond.*, **A331**, 735–800.

Villermaux, E., P. Marmottant, and J. Duplat, 2004: Ligament-mediated spray formation. *Phys. Rev. Lett.*, **92 (7)**, doi:10.1103/PhysRevLett.92.074501.

Wierzba, A., 1990: Deformation and breakup of liquid drops in a gas stream at nearly critical Weber numbers. *Exp. Fluids*, **9 (1-2)**, 59–64.

Wu, J., 1983: Sea-surface drift currents induced by wind and waves. *J. Phys. Oceanogr.*, **13 (8)**, 1441–1451.

Wu, J., 1993: Production of spume drops by the wind tearing of wave crests–The search for quantification. *J. Geophys. Res.*, **98 (C10)**, 18 221–18 227.

List of Figures

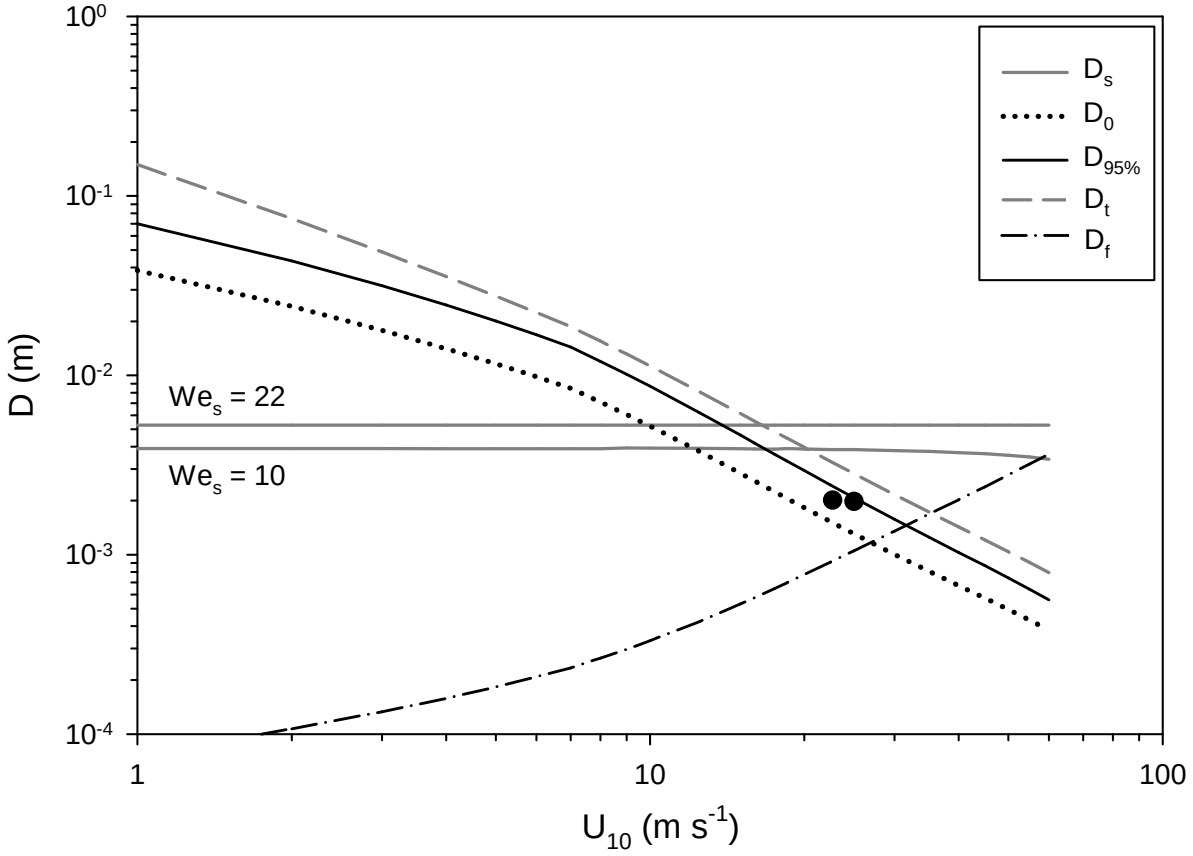

FIG. 1. The average ligament volume diameter, D_0 (dotted), maximum spray diameter, $D_{95\%}$ (solid) and maximum suspended drop size, D_f (dash-doted) are plotted as a function of wind speed. For reference, theoretical maximum diameters (dark gray) along with laboratory data points from Anguelova et al., 1999 (dots) are also plotted.

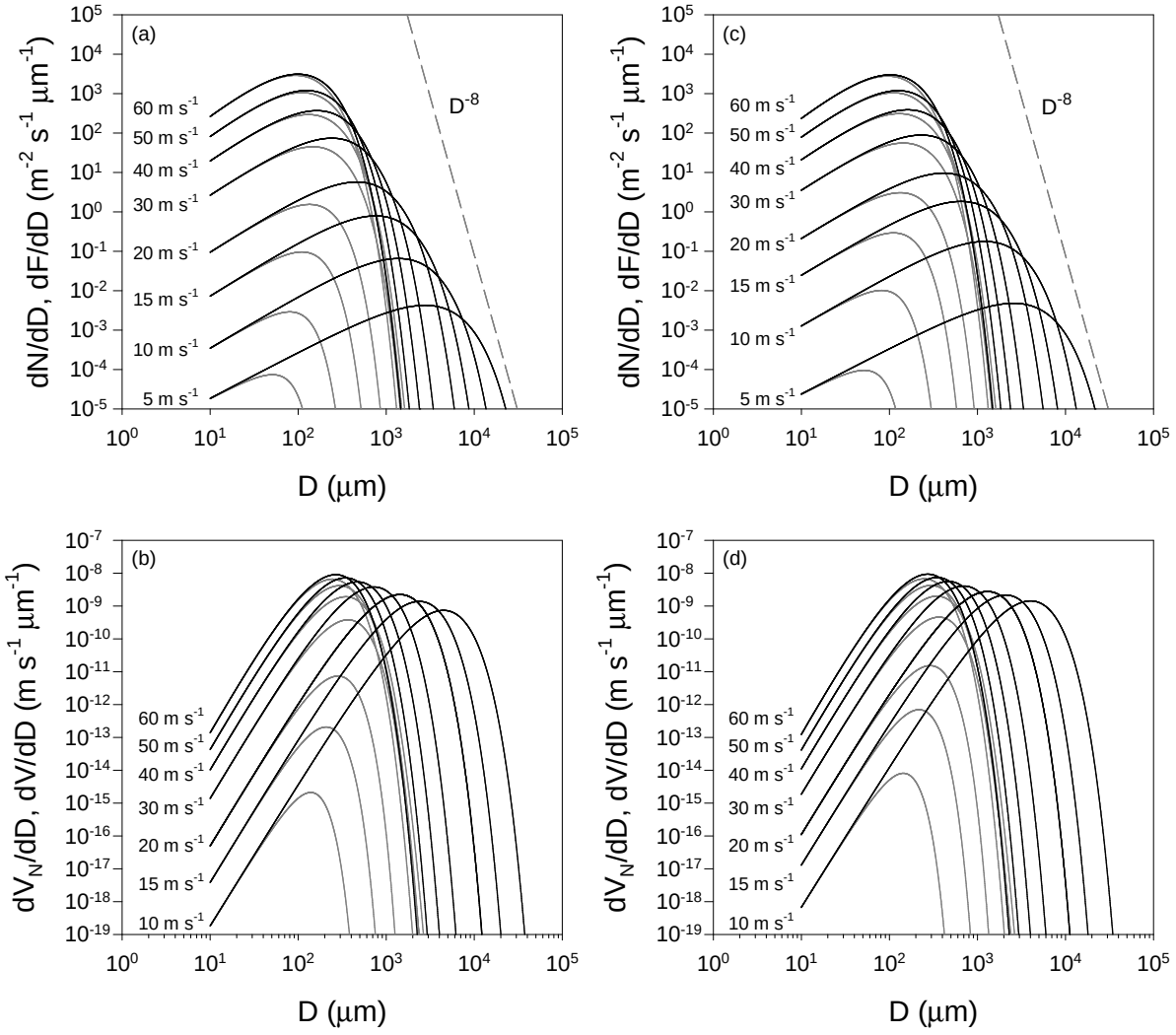

FIG. 2. The spume production functions (a,c) and associated volume distributions (b,d) along with the corresponding vertically transported quantities (gray) for multiple $10-m$ wind speeds at fetches 22 m (left) and 75 km (right)

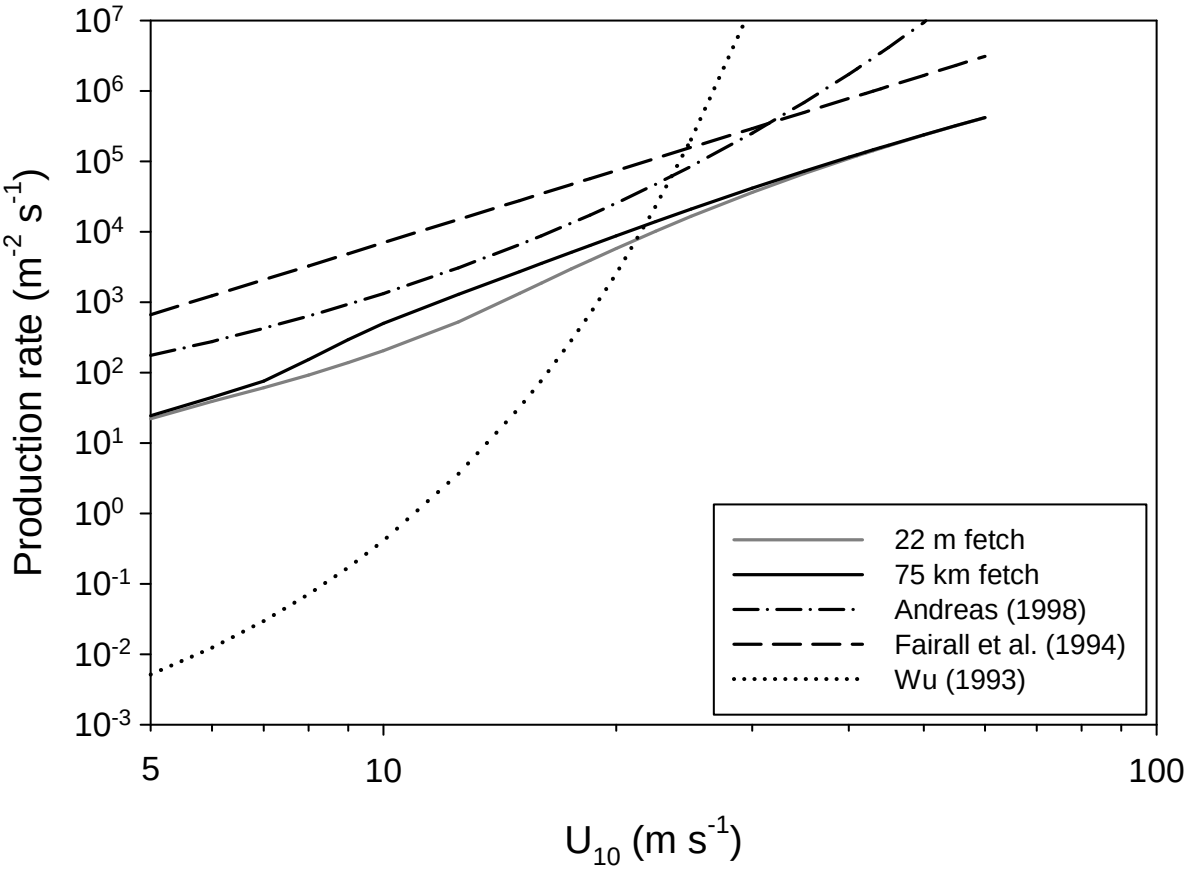

FIG. 3. The total production rate of spume drops with diameters greater than 100 μm: 75 km fetch (line), 22 m fetch (dark gray), Andreas, 1998 (dash-dotted), Fairall et al., 1994 (dashed) and Wu, 1983 (dotted)

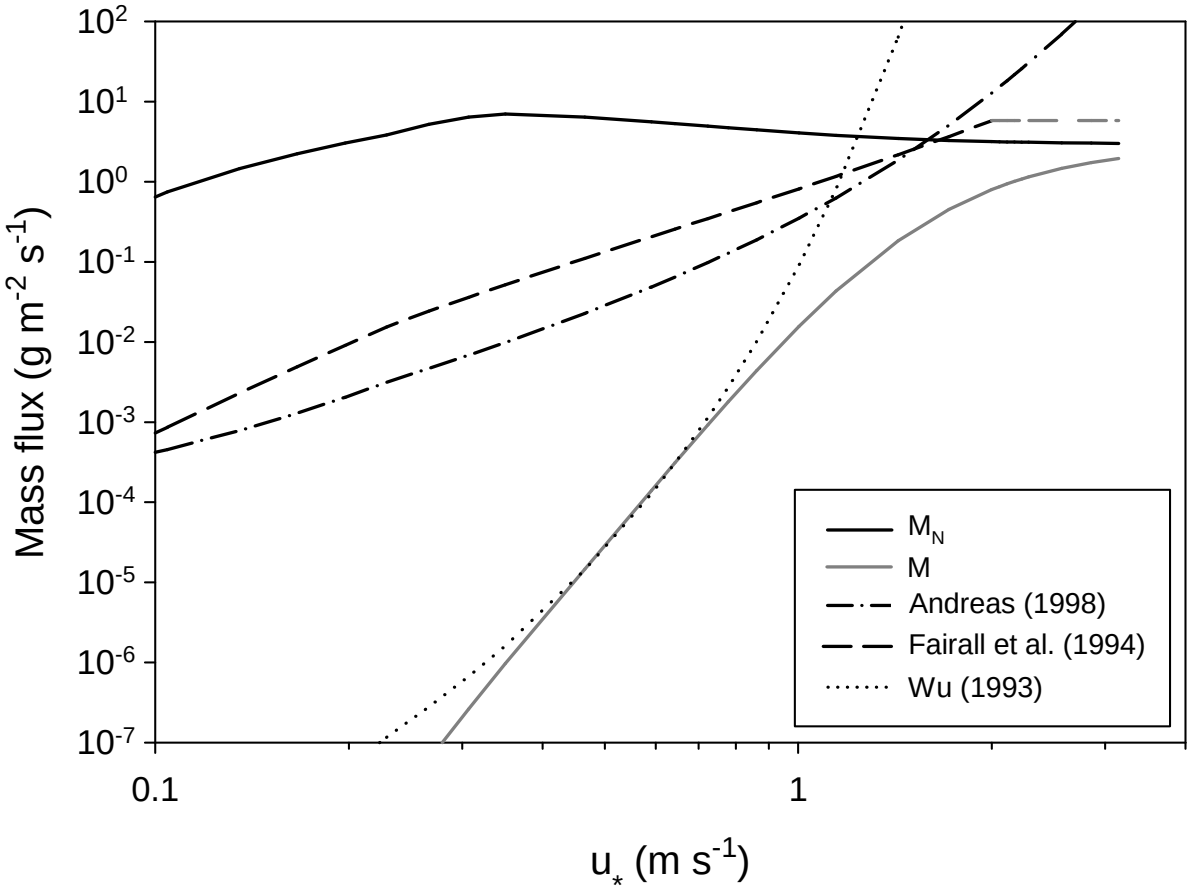

FIG. 4. Mass fluxes as a function of friction velocity: source function (line), suspended (gray), Andreas, 1998 (dash-dotted), Fairall et al., 1994 (dashed) and Wu, 1983 (dotted) along with the maximum value from Fairall et al., 1994 for 100% whitecap coverage (gray dashed)

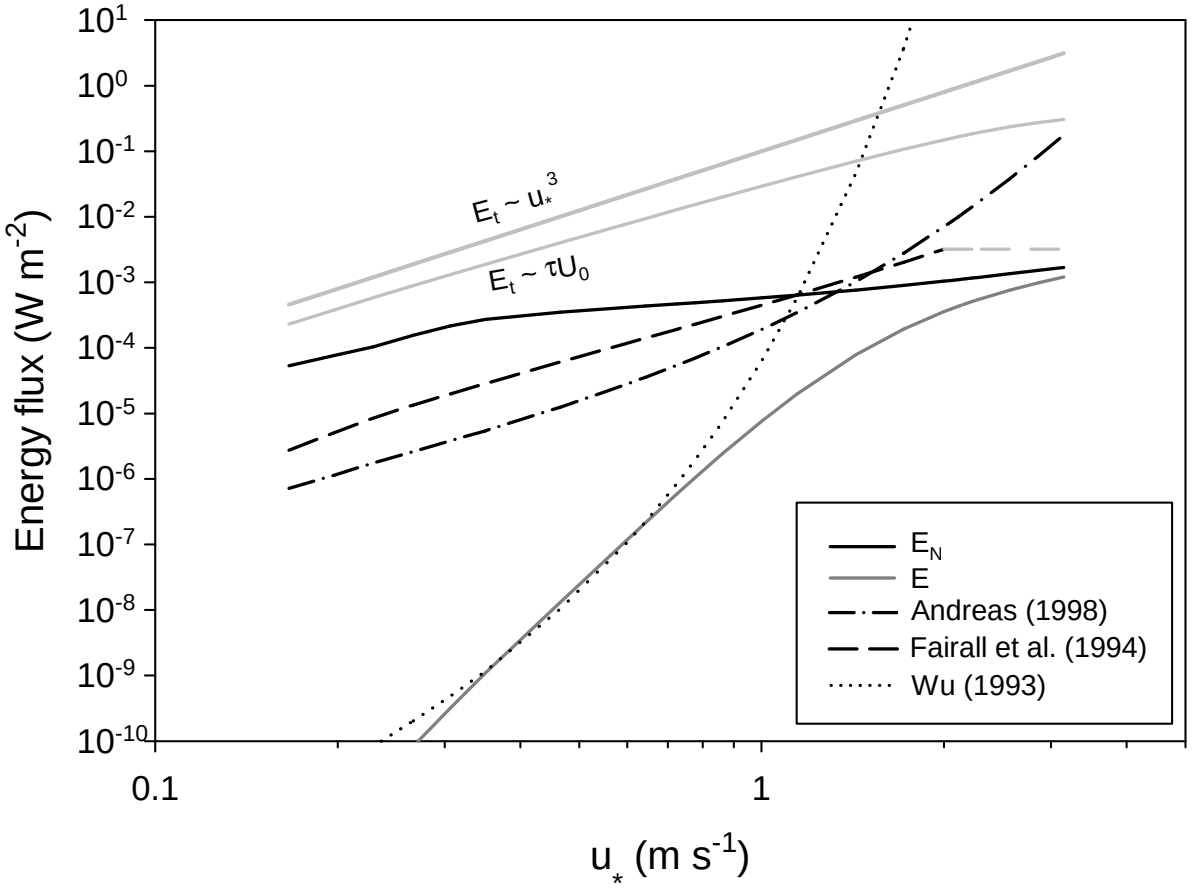

FIG. 5. Free energy as a function of friction velocity: source function (line), suspended (dark gray), Andreas, 1998 (dash-dotted), Fairall et al., 1994 (dashed) and Wu, 1983 (dotted) along with the maximum value from Fairall et al., 1994 for 100% whitecap coverage (gray dashed) and two estimates of the wind energy flux (light gray)